Room-temperature d^0 ferromagnetism in carbon-doped Y_2O_3 for spintronic applications: A density functional theory study

Brahmananda Chakraborty,[1,*] Prithwish K. Nandi,[2,†] Yoshiyuki Kawazoe,[3,4] and Lavanya M. Ramaniah[1]

[1]*High Pressure and Synchrotron Radiation Physics Division, Bhabha Atomic Research Centre, Trombay, Mumbai 400085, India*

[2]*Irish Centre for High-End Computing, Grand Canal Quay, Dublin 2, Ireland*

[3]*New Industry Creation Hatchery Center, Tohoku University, Sendai 980-8579, Japan*

[4]*Department of Nanotechnology and Physics, SRM Institute of Science and Technology, Kattankulathur 603203, India*

(Received 10 July 2017; revised manuscript received 8 March 2018; published 7 May 2018)

Through density functional theory simulations with the generalized gradient approximation, confirmed by the more sophisticated hybrid functional, we predict the triggering of d^0 ferromagnetism in C doped Y_2O_3 at a hole density of 3.36×10^{21} cm^{-3} (one order less than the critical hole density of ZnO) having magnetic moment of $2.0\,\mu_B$ per defect with ferromagnetic coupling large enough to promote room-temperature ferromagnetism. The persistence of ferromagnetism at room temperature is established through computation of the Curie temperature by the mean field approximation and *ab initio* molecular dynamics simulations. The induced magnetic moment is mainly contributed by the $2p$ orbital of the impurity C and the $2p$ orbital of O and we quantitatively and extensively demonstrate through the analysis of density of states and ferromagnetic coupling that the Stoner criterion is satisfied to activate room-temperature ferromagnetism. As the system is stable at room temperature, C doped Y_2O_3 has feasible defect formation energy and ferromagnetism survives for the choice of hybrid exchange functional, and at room temperature we strongly believe that C doped Y_2O_3 can be tailored as a room-temperature diluted magnetic semiconductor for spintronic applications.

DOI: 10.1103/PhysRevB.97.184411

I. INTRODUCTION

Introducing ferromagnetism (FM) in traditional nonmagnetic semiconductors results in diluted magnetic semiconductors (DMS) [1] which have potential applications in spintronic devices [2] because of their magnetic and magnetotransport properties. The traditional approach to design DMS is to dope $3d$ transition metals (TMs) in nonmagnetic semiconductors. When a TM is doped in TiO_2 [3,4] and ZnO [5,6] although the system exhibits ferromagnetism the exact mechanism responsible for the observed magnetic properties in TM-doped semiconductors continues to be strongly debated in the literature and it is not clear whether the induced ferromagnetism is intrinsic or not. Strong evidence of phase separation and formation of ferromagnetic clusters reported by Park *et al.* [6] in Co doped ZnO suggests extrinsic magnetic origin not suitable for technological applications [7] due to nonuniform spin density. Due to this debate there is a thrust for the search of ferromagnetic semiconductors or insulators, which are free of transition-metal or rare-earth species, called d^0 magnetism [7]. If ferromagnetism can be achieved by doping nonmagnetic elements in nonmagnetic oxide then the ferromagnetism will be definitely purely intrinsic. Another important issue for practical implementation of DMS is the persistence of ferromagnetism at room temperature. There are several studies where although induction of FM with doping at 0 K is reported there is no mention regarding stability of FM at room temperature. Doping concentration and range of ferromagnetic interactions are two important parameters to control room-temperature FM. One needs to select a particular impurity concentration where ferromagnetic coupling is large enough to promote room-temperature FM. The impurity separation at which the exchange energy vanishes gives the range $d_{\max}$ of magnetic interaction which defines the minimum concentration of impurity required to achieve room-temperature FM.

There are two established way to promote hole induced d^0 FM in nonmagnetic oxides: (i) cation vacancy or substitution of cations by a lower valency cation from group 1A or group 2A elements and (ii) anion vacancy or substitution of anions by B, N, and C elements [8,9]. Rahman *et al.* [10] predicted, using density functional theory (DFT) simulations, that a single Sn vacancy in SnO_2 introduces a magnetic moment of $4.0\,\mu_B$ by supplying four holes per vacancy in the system. But introducing vacancy in the system is not an effective way to switch on d^0 FM as the required formation energy for creating vacancy is higher compared to cation or anion substitution. Through a modified Hubbard Hamiltonian, Bouzerar and Ziman [11] theoretically predicted that the optimal situation for achieving room-temperature FM in nonmagnetic oxides requires impurities releasing three holes per defect in the system. However, recently we have predicted through DFT simulations that the room-temperature d^0 FM in SnO_2 [12] doped with impurity from group 2A elements (Be, Mg, Ca) inserts two holes per defect in the system. So, the prescription of three holes per defect is not a necessary criterion for hole induced FM, rather the system needs a critical hole concentration to activate FM.

There are many theoretical and experimental studies on room-temperature FM by introduction of holes through cation substitutions. Yi *et al.* [13] demonstrated both experimentally

*Corresponding author: brahma@barc.gov.in

†Corresponding author: prithwish.nandi@ichec.ie

and theoretically the induction of room-temperature FM in Li doped ZnO. Chawla *et al.* [14] experimentally observed FM in Li/Na doped ZnO nanorods which persists in the concentration range of 2–10 at. % and is lost for a doping concentration above 10 at. %. Ferromagnetism was also predicted in In_2O_3 through first-principles investigations when In is substituted by Li, Na, and K [15]. Substitution of Zr by K in ZrO_2 also switches on FM in nonmagnetic ZrO_2 as reported by Máca *et al.* [16]. Zhou *et al.* [17] investigated through first-principles simulations the possibility of ferromagnetism in K and Ca doped SnO_2; although they observed a magnetic moment in K doped SnO_2, the system remains nonmagnetic when doped with Ca.

Introducing holes through anion substitution or anion vacancy can also be the origin of FM in intrinsic DMS. Through DFT simulations, it has been predicted that FM can be triggered in nonmagnetic group-II oxides MO (M = Mg, Ca, Sr, Ba) by substituting O with C or N [18–20]. It was demonstrated by Elfimov *et al.* [20] that the substitution of nitrogen for oxygen in simple nonmagnetic oxides leads to holes in N $2p$ orbitals resulting in local magnetic moments. Wu *et al.* [21] demonstrated through DFT simulations the induction of FM in C or N doped MgO and ZnO. Even though the mechanism of ferromagnetism was outlined the Curie temperature was not mentioned and it was not clear whether FM persists up to room temperature or not. Ferromagnetism in C doped ZnO was predicted by Pan *et al.* [7] with a Curie temperature higher than 400 K through DFT simulations which were demonstrated by experiment. Zhou *et al.* [22] have provided the experimental evidence of room-temperature FM in C doped ZnO when concentration of impurity exceeds a certain limit. In addition, C doping can also alter the optical properties of the host material. Liu *et al.* [23] reported that C doping can act as a color center and tunes the optical properties of various host materials.

The hole induced d^0 FM was also reported in defected SiC and carbon related materials. Wang *et al.* observed long-range ferromagnetic coupling in defected SiC [24] through experiment and also support from DFT simulations. Through first-principles simulations, Zhao *et al.* investigated the roles of silicon vacancy and nitrogen impurity in the magnetic properties of silicon carbide [25]. They observed a stable ferromagnetic ordering with a magnetic moment of 2.0 μ_β per Si vacancy when the N : V_{Si} ratio is near 2:1. Room-temperature FM in a fluorinated silicon carbide nanotube was also predicted by Lou [26] through DFT simulations. Transition-metalfree FM was also reported in some carbon systems [27–31] and it was predicted that intrinsic carbon defects could be responsible for the observed magnetic properties. Carbon adatoms in carbon nanotubes [32] and carbon substitutional doping in boron nitride nanotubes were predicted to switch on magnetic signatures in the respective systems.

Although there are controversies and difficulties in the practical realization of TM-doped DMS, d^0 FM (free from transition metal) has been successfully implemented experimentally in various nonmagnetic oxides, e.g., Li doped ZnO [13], C doped ZnO [7], Li/Na doped ZnO nanorods [14], C implanted ZnO [22], etc. But so far there is no study on anion substitution of Y_2O_3 and only recently we have reported room-temperature FM in Y_2O_3 [47] due to cation substitution (Li, Na, and K in place of Y) through DFT simulations. Yttria is an industrially and technologically handy ceramic material and the cubic structure is stable at room temperature and ambient pressure. It is reported [1] that for binary semiconductors with shorter bond length and wider band gap Curie temperature T_c is higher. So, it is worthwhile to explore the possibility of room-temperature FM in Y_2O_3 through substitution of anion O by C.

Even though there exist many studies on induction of FM in nonmagnetic semiconductors by substitution of *sp*-type impurities, the theoretical predictions are quite method dependent and the exact mechanism responsible for the induced FM continues to be strongly debated in the literature. Also, the predictions through density functional theory simulations are sensitive to the method, especially the choice of exchange-correlation functionals. When local-density approximations (LDA) or generalized gradient approximations (GGA) are used then the impurity $2p$ band becomes too extended and the prediction of magnetism gets overestimated. As LDA or GGA cannot estimate the accurate band gap, the relative position between the Fermi level and the impurity band remains uncertain, which has a very strong impact on the induced magnetism. A hybrid functional [Heyd-Scuseria-Ernzerhof (HSE06)] [33] as exchange-correlation functional is known to describe the band gap and the magnetic configuration in a much better way. So, we have used a state-of-the-art hybrid functional, based on the HSE06 functional [34], to confirm the magnetic moment and density of states (DOS) predicted by GGA simulations.

Another important issue is the stability of the system. For practical implementation of DMS in spintronic devices the system should be stable at room temperature with persistence of FM. The impurity should not move out of the system and there should not be impurity-impurity clustering. There exist reports where induction of hole doped FM has been studied without checking the stability of the system. We have taken care of these practical issues very carefully and checked the stability of the system through *ab initio* MD simulations and computed the formation energy of impurity. As we have considered a state-of-the-art hybrid functional, based on the HSE06 functional [34], along with GGA exchange correlations, we have checked the stability of the system and persistence of FM at room temperature, and we have computed the formation energy of impurity, we strongly believe that C doped Y_2O_3 can be practically implemented as room-temperature DMS in spintronic devices.

In this paper, through density functional theory simulations, we predict the triggering of d^0 ferromagnetism in C doped Y_2O_3 having magnetic moment of 2.0 μ_B per defect with ferromagnetic coupling large enough to promote room-temperature ferromagnetism. The persistence of ferromagnetism at room temperature is established through computation of the Curie temperature by the mean field approximation (MFA) and *ab initio* MD simulations.

II. COMPUTATIONAL DETAILS

All the spin-polarized calculations (ionic relaxation, electronic structure, and *ab initio* MD simulations) were carried out within the framework of DFT, using the projector augmented wave (PAW) method for the core-valence

interaction as implemented in the VASP code [35–38]. In order to describe the exchange-correlation functional, we employ the generalized gradient approximation as implemented by Perdew, Burke, and Ernzerhof (PBE) [39] along with an energy cutoff of 500 eV for the plane-wave basis expansion. PBE is known to successfully predict the geometries of transition-metal complexes and magnetic systems over other varieties of GGA [40]. The valence configurations for Y, C, and O in the PAW pseudopotentials were taken as $4s^2 4p^6 4d^1 5s^2$, $2s^2 2p^2$, and $2s^2 2p^4$, respectively. We have taken the cubic structure of yttria, which is stable at room temperature and ambient pressure, and the supercell contains 32 yttrium and 48 oxygen atoms in a cube of length 10.75 Å. The self-consistent field convergence threshold was taken as 10^{-5} eV, while the Hellmann-Feynman forces were less than 0.01 eV/Å in the structural optimization. A Monkhorst-Pack [41] grid was used for the sampling of the Brillouin zone and $6 \times 6 \times 6$ K-points are considered for accurate computations of DOS. We have repeated some of the calculations with state-of-the-art hybrid functional calculations based on the HSE06 functional [34] to check our GGA results. To check the stability of the structure and persistence of FM at room temperature, *ab initio* MD simulations are carried out at 300 K within the canonical *NVT* ensemble with Γ-point sampling and Nośe thermostat [42].

III. RESULTS AND DISCUSSION

A. Structure and magnetic moment

The optimized structures of yttria doped with a single C atom (in place of O) and doped with double C atoms are displayed in Fig. 1. Yttria is a nonmagnetic band insulator with Mn_2O_3 bixbyite structure having space group *Ia3*-(T_h^7) and the unit cell contains two inequivalent cation (Y^{3+}) sites, 8*a* (say, Y1) and 24*d* (say, Y2), and one type of anion (O^{2-}) positioned at 48*e* sites. Our computed lattice constant ($a = 10.74$ Å) for perfect bulk yttria matches nicely with the corresponding experimental value of 10.604 Å as given by Wyckoff [43]. In perfect yttria, the O atom is linked to one Y1 and three Y2 atoms in the form of a distorted tetrahedron whereas Y is bonded with six O atoms having equal bond lengths of 2.305 Å with nearest Y-Y separation of 3.554 Å. When O is substituted with C, the Y-C bond length increases by 4% compared to corresponding Y-O bond length due to outward relaxation of the anion. Here we note that although there is weakening of the bond the symmetry of the structure is preserved. With single impurity in the supercell, which corresponds to an impurity concentration of 2.08 at. %, the FM is triggered in the nonmagnetic host with magnetic moment of 2.0 μ_β. When O is replaced by C, it incorporates two holes in the system and the expected magnetic moment is 2.0 μ_β; interestingly we have obtained exactly the same value. We have considered two different impurity concentrations of 2.08 and 4.16 at. % by introduction of single and double impurities in the simulation cell, respectively.

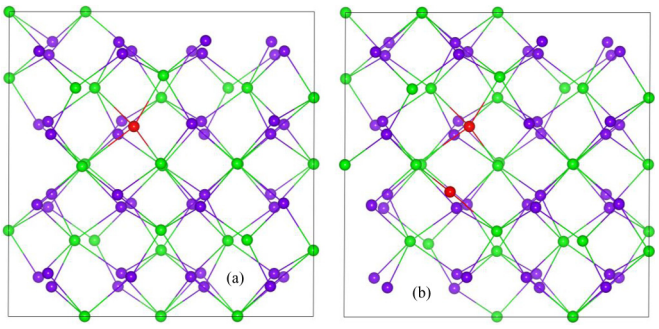

FIG. 1. Relaxed structure of C substituted Yttria with impurity concentration of (a) 2.08 at. % and (b) 4.16 at. %; green, purple, and red atoms are Y, O, and C, respectively.

Though it is observed that doping of C does introduce local magnetic moments in yttria, it is necessary to understand how these local moments interact among themselves with increasing impurity concentration. We can pose two fundamental questions.

(i) How does the magnitude of total magnetic moment change with impurity concentration?

(ii) What is the possible mechanism of the interaction between these local moments?

While the answer to the first question helps us to get a quantitative idea of the variation of magnitude of total moment with impurity concentration, the second question essentially relates to the qualitative scenario describing how the isolated local moments align themselves to result in a ferromagnetic order with a net moment. Here, we have studied four different cases where the impurity C atoms are kept at four different distances: case 1, $d = 1.37$ Å; case 2, $d = 3.37$ Å; case 3, $d = 4.51$ Å; and case 4, $d = 4.78$ Å. Please note that, for C, the single impurity induces a net moment of 2.0 μ_B (say, M_s), and as concentration is doubled the net moment is seen to be almost equal to $2 \times M_s$ except the case where the two impurity atoms are close enough (at $d = 1.37$ Å) to quench the net moment to zero. So, with increasing impurity concentration there is linear scaling of magnetic moment, except for very low concentration, which is a positive indicator for practical applications in spintronic devices as enhanced magnetic moment can be obtained by increasing the density of the impurity in the system. Therefore, we can see that doping of Y_2O_3 with C with impurity concentration as low as 2.08 at. % may be a possible way of tailoring Y_2O_3 based DMS.

B. Analysis through density of states and partial density of states

Now we will focus on spin resolved DOS for C doped Y_2O_3 in order to shed some light on the mechanism of induced ferromagnetism. In our earlier work [47], we have reported that for pure yttria a GGA computed band gap of 4.224 eV, although it reasonably matches with a linear muffin-tin-orbital method based band gap of 4.54 eV by Mueller *et al.* [44], is much lower than the experimental value of 5.8–6 eV [45,46]. Then we employed a state-of-the-art hybrid functional based on the Heyd-Scuseria-Ernzerhof functional and obtained a band gap of 5.6 eV, nearer to the experimental band gap. So here also we have verified the GGA result with the results obtained with the hybrid functional (HSE06). Figure 2 displays the total DOS for C doped (in place of O) yttria with GGA [left panel Fig. 2(a)] and with the hybrid functional [right panel Fig. 2(b)].

Due to introduction of holes, there appear narrow highly localized impurity bands exhibiting an obvious spin split around

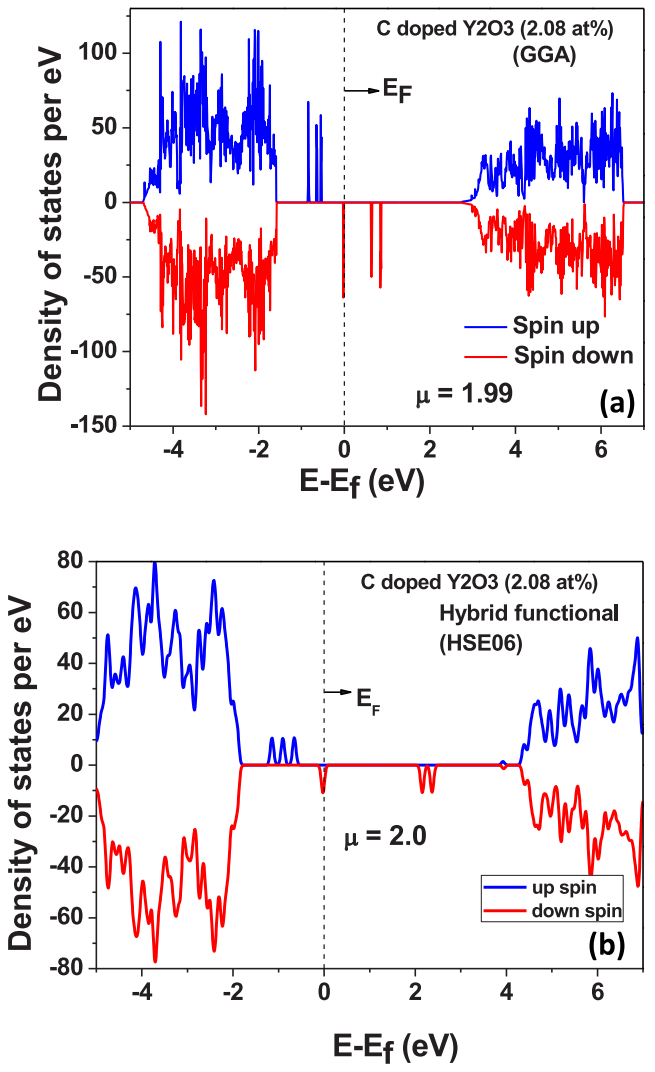

FIG. 2. Spin resolved total density of states for C substituted (in place of O) Y_2O_3 with (a) GGA exchange functional and (b) hybrid functional HSE06.

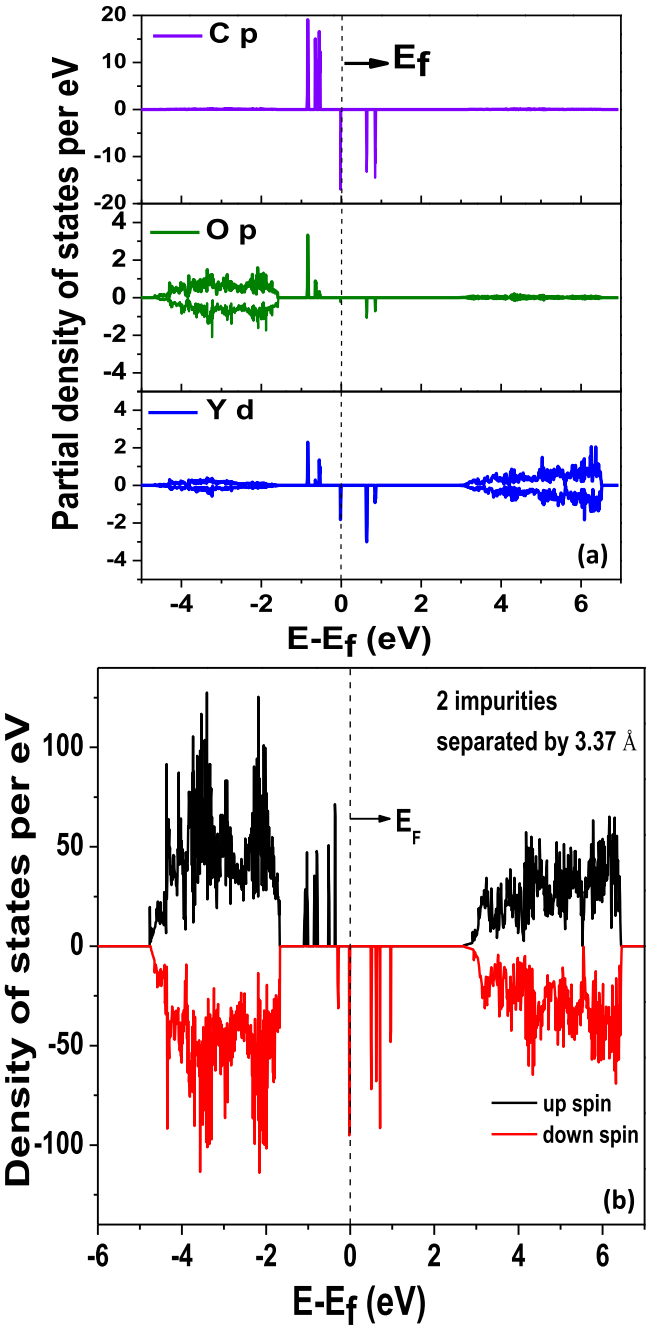

FIG. 3. (a) Spin resolved partial density of states (PDOS) for dopant $2p$ orbital (upper panel), O $2p$ orbital (middle panel), and Y $4d$ orbital (lower panel). (b) Spin resolved total density of states with two impurities in the supercell (impurity concentration 4.16 at. %) separated by a distance of 3.37 Å.

the Fermi level as seen in Fig. 2(a) signifying the induced FM for carbon substituted Y_2O_3. We observe three up-spin levels and three down-spin levels due to this spin splitting. All the up-spin channels are fully occupied whereas one down-spin channel is partially occupied and the other two are unoccupied. The energy separation $\Delta E1$, between the maximum of the split up-spin channel and the maximum of the split down-spin channel, is 1.547 eV, whereas the energy separation $\Delta E2$, between the minimum of the split up-spin channel and the minimum of the split down-spin channel, is 0.77 eV. So, we can see that a single electron in the p orbital causes the energy splitting between the up-spin and down-spin channels, making C doped yttria a dilute magnetic semiconductor. The DOS computed using the hybrid functional (HSE06) as displayed in Fig. 2(b) also portrays similar features with three up-spin levels and three down-spin levels around Fermi level with net magnetic moment of 2.0 μ_β. The only difference is that now impurity states are a little broader and the separation between down-spin levels is wider. So, the hole induced FM was also observed using the hybrid functional, which is supposed to provide more accurate description of DOS and magnetic properties.

In order to find the contribution of magnetic moment among different elements present in the system in Fig. 3(a) we have plotted the projected density of states (PDOS) of the p orbital of impurity C, the p orbital of the O atom close to the impurity, and the d orbital of the Y atom. We can notice that the magnetic moment is mainly contributed by the dopant p orbital while

the p orbital of surrounding O atoms and the d orbital of the four bonded Y atoms also contribute a little bit to the induced magnetism. A deep impurity band is pushed up in the band-gap region and the system exhibits hybridization between the dopant p orbital, O p orbital, and Y d orbital. The interaction causes the energy splitting between the up-spin channel and the down-spin channel. From the PDOS analysis it appears that p-d hybridization is stronger than p-p hybridization. We have computed the contribution of the magnetic moment for each ion in this hole doped system. Out of $2.0\,\mu_\beta$, due to introduction of a single impurity in the system, the impurity ion contributes around 60% of the magnetic moment whereas the remaining contribution comes from nearest O ions and nearest Y ions. So, the magnetic moment is not much extended as in the case of cation substituted Y_2O_3 [47]. Here we note that the impurity, cation Y, and anion O are magnetically aligned in the same direction contrary to the case of cation substituted Y_2O_3 and SnO_2 where the cations are magnetically antiparallel to the anion O. So, the impurity plays the more crucial role to induce FM in the system as it not only instigates spin splitting by tuning the Fermi level but also contributes the major part of induced magnetic moment. Figure 3(b) displays the total DOS with two impurities placed at a separation of 3.37 Å, which corresponds to a doping concentration of 4.16 at. %. Due to two impurities we can see more defect states resulting in a magnetic moment of $4.0\,\mu_\beta$.

C. Bader charge analysis

We have performed a complete Bader charge analysis to assess the charge transfer due to introduction of impurity. In perfect Y_2O_3, the yttrium site acts as a cation whereas the oxygen site acts as an anion with an excess charge of $1.4301e$ per oxygen site according to Bader partitioning. When C is introduced in the O site, there are two holes in the system resulting in a redistribution of the charge. Four Y ions bonded with the impurity gains around $0.07e$ of charge each. In order to balance it there is charge transfer from impurity C as well as nearest O ions. The impurity C transfers charge of around $0.1417e$ whereas nearest O ions gives around $0.018e$ charge each. In the course of the charge transfer, the charge of opposite spin does not come in the same proportion leading to spin polarization in the nonmagnetic Y_2O_3. As the charge transfer from the impurity ion is highest it has maximum contribution for the induced magnetic moment, consistent with the computation of magnetic moment for each ions described earlier. Similarly O ions and Y ions have less contribution in the induced magnetic moment due to less amount of charge transfer.

D. Spin-density analysis

Figures 4(a) and 4(b) display the real-space plot of the effective spin density (from GGA) obtained by taking the difference between the charge densities of majority and minority spins ($\Delta\rho = \rho\uparrow - \rho\downarrow$) for isovalues of $0.03e$ and $0.0075e$, respectively with a single impurity in the supercell (impurity concentration of 2.08 at. %). We can notice from Fig. 4(a) that the effective spin density is mainly concentrated on the impurity atom. There is also a little contribution from nearest-neighbor Y atoms and the next-nearest-neighbor O atoms as seen from Fig. 4(b) for a lower isovalue of $0.0075e$ signifying

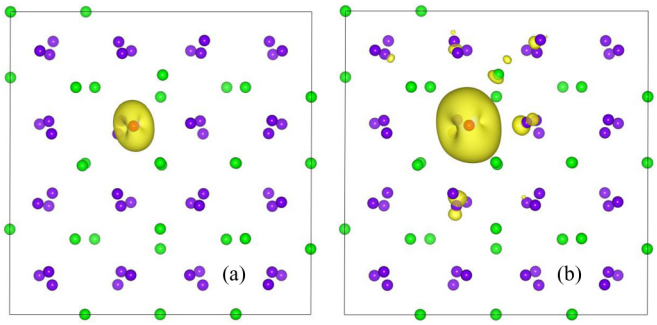

FIG. 4. The real-space plot of the effective spin density obtained by taking the difference between the charge densities of majority and minority spins ($\Delta\rho = \rho\uparrow - \rho\downarrow$). Spin-density isosurface for C doped Y_2O_3 (2.08 at. %) for (a) isovalue $0.03e$ and (b) isovalue $0.0075e$; Y atoms are in green, O atoms are in purple, C atoms are in orange, and spin-density isosurfaces are presented in yellow and are mostly concentrated around the impurity atom and a little bit around the first shell O atoms.

the extended nature of the spatial distribution of spin moments. The total area of the isosurface presents a qualitative indication of the magnetic moment. The spin-density plot is qualitatively consistent with the PDOS analysis and computation of magnetic moment contribution by each atom. Figure 5 portrays the spin-density isosurface for isovalue of $0.03e$ and $0.0075e$ when two impurities are placed in the supercell which corresponds to impurity concentration of 4.16 at. %. We can see that for higher impurity concentration the magnetic moment is more extended due to ferromagnetic interaction. The spin-density isosurfaces look like dumbbell shape as the magnetic moment in this system is mainly originated from p orbitals.

E. *Ab initio* MD simulations

We have carried out *ab initio* MD simulations at 300 K to check the stability of the structure and the sustainability of the ferromagnetism at room temperature (also predicted by MFA through computation of T_c discussed in the next section).

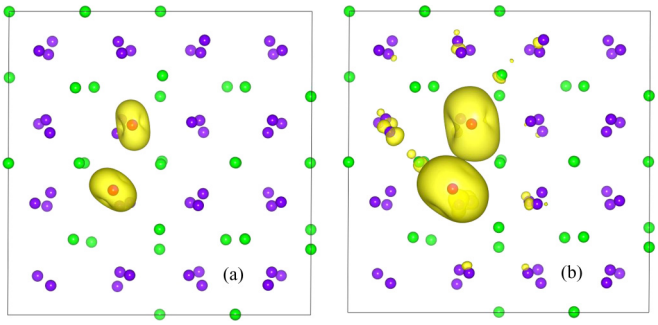

FIG. 5. The real-space plot of the effective spin density obtained by taking the difference between the charge densities of majority and minority spins ($\Delta\rho = \rho\uparrow - \rho\downarrow$). Spin-density isosurface with two impurities in the supercell for C doped Y_2O_3 (4.16 at. %) for (a) isovalue $0.03e$ and (b) isovalue $0.0075e$; Y atoms are in green, O atoms are in purple, C atoms are in orange, and spin-density isosurfaces are presented in yellow and are mostly concentrated around the impurity atom and a little bit around the first shell O atoms.

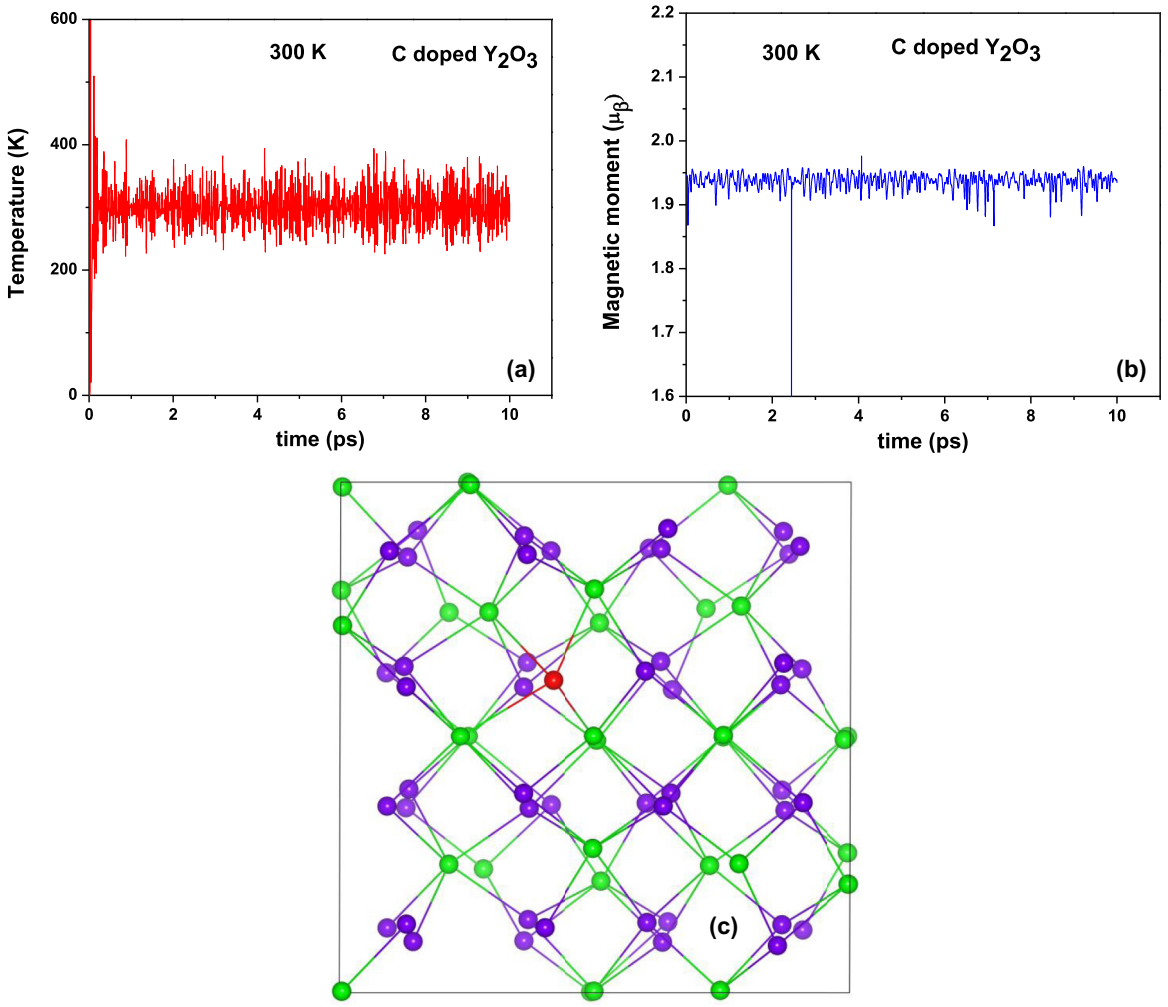

FIG. 6. The fluctuation of (a) temperature and (b) ferromagnetic moment as a function of molecular dynamics simulation steps at 300 K for C doped yttria. (c) Structure of C doped yttria at 300 K showing the stability of the system at higher temperature.

Figures 6(a) and 6(b) show, respectively, the fluctuation in temperature and fluctuation in magnetic moment as a function of simulation time for C doped yttria at 300 K. After 10 ps, we observe that the structure remains stable and the ground state is still ferromagnetic with an average magnetic moment of 1.9476 μ_β, which is close to the value obtained through DFT simulations. Figure 6(c) portrays the structure of C doped yttria at 300 K showing the stability of the system at higher temperature. This implies that the binding energies of C-Y and C-O are higher than the thermal energy corresponding to the room temperature. The MD simulation carried out over 10 ps shows very small fluctuation in magnetic moment signifying that C doped yttria is stable room-temperature DMS.

F. Computation of T_c using mean field approximation

In order to check the persistence of FM at room temperature we have computed the Curie temperature T_c employing the MFA where, T_c is expressed for a given concentration as $T_c = \frac{2}{3} z j(\bar{r})$, where $j(\bar{r})$ is the exchange coupling constant corresponding to the average separation distance $\bar{r}$ containing z number of nearest neighbors [48]. The exchange coupling $j(\bar{r})$ is proportional to ΔE, the energy difference between the FM and antiferromagnetic (AFM) configurations [49].

We have studied four different cases where the impurity C atoms are kept at four different distances: case 1, $d = 1.37$ Å; case 2, $d = 3.37$ Å; case 3, $d = 4.51$ Å; and case 4, $d = 4.78$ Å. Figure 7 displays the energy difference between the FM and AFM as a function of impurity separation. It is clear from Fig. 7 that with increasing impurity separation ΔE decreases towards zero and the variation pattern is similar to Li, Na, and K doped Y_2O_3 [47] and defects in CaO by Osorio-Guillén *et al.* [50]. We have followed the procedure mentioned in Rahman *et al.* [10] and in Zhao *et al.* [48] and calculated the exchange energy J from ΔE by taking all neighboring spins including the spin from periodic images of the supercell especially when the impurities are placed at larger separations. The range of magnetic interaction, $d_{\max}$, is defined as the separation at which the exchange energy vanishes. The value of $d_{\max}$ decides the minimum concentration of defects needed to achieve room-temperature ferromagnetism. From the variation of ΔE in Fig. 7, we can say that the range of the magnetic interaction is less than half the cell length (~4.75 Å) and the supercell considered here is sufficient to include all magnetic interactions. One positive feature of having larger magnetic interaction range is that the system needs a lower defect concentration to achieve room-temperature ferromagnetism.

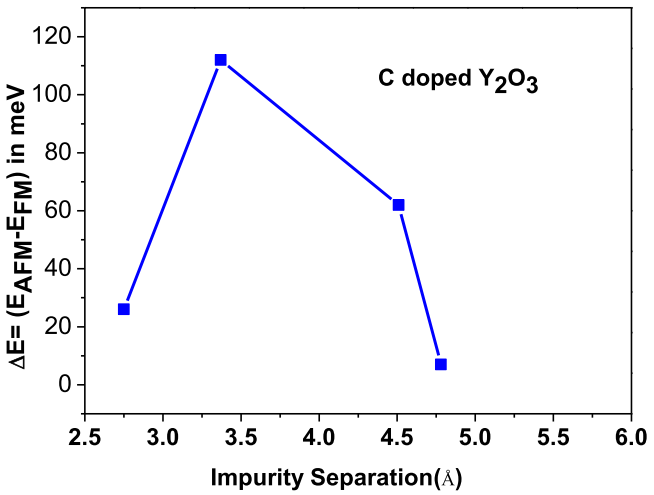

FIG. 7. Variation of ΔE, the energy difference between the antiferromagnetic (AFM) and ferromagnetic (FM) configurations with impurity separation for C doped yttria.

In the case of C doped Y_2O_3, the coupling is ferromagnetic at all separations and the computed T_c is around 675 K, higher than room temperature. Ferromagnetic coupling in all configurations is also observed in alkali-doped In_2O_3 [15]. Here, we mention that in the case of C doped Y_2O_3 the energy difference ΔE is larger than in the case of Cu doped ZnO (42 meV), which is known to be ferromagnetic at room temperature [49]. In spite of the fact that the mean field approximation overestimates T_c, we can say that for C doped Y_2O_3 the FM persists at room temperature, as computed T_c (675 K) is much higher than the room temperature (300 K). Hence our detailed simulations results can predict that tailoring of room-temperature d^0 magnetism can be achieved in a nonmagnetic host Y_2O_3 by doping C which introduces two holes per defect. Regarding the computation of T_c using mean field approximation here we mention that MFA is known to often overestimate T_c. MFA provides better results for higher impurity concentrations. Kudrnovsky *et al.* [51] compared experimental data with MFA data for GaMnAs up to Mn concentration of 2.08 at. % and reported that the agreement improves with increasing Mn concentration and it is in fair qualitative agreement around 2.08 at. %. In C doped Y_2O_3, we have used the MFA method for 4.16 at. %, which is considered to be a reasonably good concentration compared to the experimentally attainable impurity concentrations, and expect it to be not far away from the experimental value. Bouzerar [52] compared the Curie temperature for DMS obtained by MFA, RPA, and Monte Carlo methods and predicted that for DMS T_c computed using MFA matches nicely with T_c estimated by RPA and Monte Carlo methods. So, from the support of the above two works, we believe that although MFA gives an upper estimate of T_c, it is not far away from the experimental value in this case.

G. Mechanism for magnetism

From our analysis of PDOS and spin-density plot it is clear that the induced magnetic moment is due to introduction of holes in the system and mainly contributed by the $2p$ orbital of the impurity C and the $2p$ orbital of O. We know that in solids the origin of magnetism is due to the presence of highly localized unpaired electrons in $3d$ and $4f$ states of the transition and rare-earth metals. Interestingly, the $2p$ electrons of the second row elements B, N, and C have similar properties to $3d$ orbitals of transition metals [53,54].The radial wave function of $2p$ orbitals of C and O have a similar localized nature to $3d$ orbitals of Mn and their spin splitting energy is higher than Mn $3d$ orbitals [53,54]. Due to the localized nature of $2p$ orbitals of C and O and large spin splitting energy it is possible to switch on spin polarization in a nonmagnetic host Y_2O_3 by introducing holes around the O atoms. The introduction of localized magnetic moments in C doped yttria depends on the relative strength of the electronegativity of the dopant element and the anion O. A weaker bond between the cation and the dopant leads to a localized atomiclike $2p$ orbital of the dopant and a stable spin-polarized state whereas a stronger bond results in delocalization of the dopant $2p$ orbitals due to strong hybridization of the cation and introduces reduced or vanishing spin polarization in the system [55]. In perfect yttria, Y-O bond length is 2.28 Å whereas the bond length is increased to 2.42 Å for C doped yttria. So, when O is replaced by a smaller electronegativity element, say C, a spin-polarized defect band is introduced which can then mediate the magnetic interaction through a double exchange mechanism [53]. But it requires fine tuning to satisfy the Stoner criterion [53] as predicted by the band picture model for the emergence of ferromagnetism. According to the band picture model, for spontaneous FM, the relative gain in exchange interaction energy is larger than the loss in kinetic energy, i.e., the Stoner criterion should be satisfied, i.e., $D(E_F)\,J > 1$, where $D(E_F)$ is the density of states at the Fermi level and J is the strength of the exchange interaction [53]. Now we try to demonstrate quantitatively and extensively through the analysis of the density of states and ferromagnetic coupling whether the Stoner criterion is satisfied or not for C doped Y_2O_3. When two C impurities are separated by 3.37 Å, $D(E_F)$ is 95.2 per eV as seen from Fig. 3 and $J \sim 0.112$ eV; so $D(E_F)$. $J = 95.2 \times 0.112 = 10.66 > 1$, which satisfies the Stoner criterion and induces FM in the nonmagnetic Y_2O_3 with the ferromagnetic coupling large enough to sustain magnetic signature at room temperature. Here ferromagnetism is turned on at a hole concentration of $1.63 \times 10^{21}\,\mathrm{cm}^{-3}$, which is almost one order less than the critical hole density of ZnO, $2.76 \times 10^{22}\,\mathrm{cm}^{-3}$ [43], and less than group1A impurity (Li^+, Na^+, K^+) doped SnO_2 [12].

H. Practical feasibility

In order to assess the practical realization of C doped Y_2O_3 as room-temperature DMS, we have computed the various defect formation energies. When C is doped on Y_2O_3, there are various types of defect configurations: (i) oxygen substitution defect, (ii) interstitial defects, and (iii) Y substitution defects.

First we have computed the formation energy of Y_2O_3 from metallic Y and O_2 gas using the formula [56]

$$\begin{aligned} E_{\mathrm{form}}^{Y_2O_3} &= 2\mu_Y^{Y_2O_3} + 3\mu_O^{Y_2O_3} - \left(2\mu_Y^0 + 3\mu_O^0\right) \\ &= E_{Y_2O_3} - \left(2\mu_Y^0 + 3\mu_O^0\right), \end{aligned} \quad (1)$$

where $E_{Y_2O_3}$ is the energy per molecule of pure Y_2O_3; $\mu_Y^{Y_2O_3}$ and $\mu_O^{Y_2O_3}$ are the chemical potential of Y and O in Y_2O_3, respectively; μ_Y^0 is the chemical potential of Y in pure yttrium metal; and μ_O^0 is the energy of pure O_2 gas (per oxygen atom). The computed formation energy using the GGA exchange-correlation function is

$$\begin{aligned} E_{\text{form}}^{Y_2O_3} &= E_{Y_2O_3} - \left(2\mu_Y^0 + 3\mu_O^0\right) \\ &= -46.24 - (2 \times -6.275 + 3 \times -9.54/2) \\ &= -19.38\,\text{eV}. \end{aligned}$$

This is in good agreement with the reported theoretical value of −19.41 eV [56] and experimental value of −19.62 eV [57]. The reasonable matching of formation energy with reported experimental and simulated value gives us confidence regarding the correctness of the simulation procedure and the methods. From stability criteria, the range of $\mu_Y^{Y_2O_3}$ is given by [56]

$$\mu_Y^0 + \tfrac{1}{2}E_{\text{form}}^{Y_2O_3} < \mu_Y^{Y_2O_3} < \mu_Y^0. \tag{2}$$

We have considered the value of $\mu_Y^{Y_2O_3}$ in the above range ($-15.97 < \mu_Y^{Y_2O_3} < -6.275$ eV) for computing the defect formation energy.

We now try to compute the chemical potential of C. For that we need to compute the energy of a single C atom in some C compound. In the literature, the chemical potential of C has been computed taking the energy of a single carbon atom from various C sources. Berseneva *et al.* [58] have taken μ_c as the energy of a single C atom in graphene. Di Valentin *et al.* [59] computed μ_c from CO_2. Lu *et al.* [60] considered energy of an isolated C atom as μ_c. Atanelov *et al.* [61] calculated μ_c with respect to C in diamond. Following the work of Berseneva *et al.* [58] we have taken μ_c as the energy of a single C atom in graphene. Here we mention that the choice of carbon source does not change the relative stability between substitutional and interstitial defects. The relative formation energy is the main concern in this paper and the absolute formation energy may not be very relevant to the experimentalist while synthesizing C doped Y_2O_3 as it depends on experimental conditions as well as the source materials used for the growth.

The computed energy for a graphene sheet of 32 atoms using the GGA exchange-correlation function is −295.6 eV, which gives $\mu_c = -9.2$ eV. To check the correctness of this value, we have computed the cohesive energy of graphene per atom using the formula

$$E_c = \left(E_{\text{grph}} - N \times \mu_c^0\right)/N, \tag{3}$$

where E_{grph} is the energy of a graphene sheet with N carbon atoms and μ_c^0 (−1.33 eV, our computed value) is the energy of an isolated C atom. The computed cohesive energy comes out to be −7.91 eV, which matches very nicely with the DFT computed literature value of −7.92 eV [62]. Using $\mu_c = -9.2$ eV, the formation energy for interstitial carbon doping comes out to be 7.46 eV. This formation energy is close to the formation energy of ∼8 eV for interstitial carbon doping in TiO_2 [59].

Oxygen chemical potential is the parameter which can be tuned in the experiment by changing the temperature and O_2 pressure following the relation [63]

$$\mu_0(T,P) = \mu_0(T,P_0) + \frac{1}{2}KT \times \ln\left(\frac{P}{P_0}\right), \tag{4}$$

where $P_0 = 1$ atm.

From the stability criteria, the range of O chemical potential is given by [64]

$$\mu_O^0 + \tfrac{1}{3}E_{\text{form}}^{Y_2O_3} < \mu_O^{Y_2O_3} < \mu_O^0. \tag{5}$$

Here, μ_O^0 is defined as $\mu_O^0 = \frac{1}{2}E_{O2} = -4.77$ eV (from our calculation, $E_{O_2} = -9.54$ eV). So from Eq. (5), the O-rich case corresponds to $\mu_0{}^{Y_2O_3} = \mu_O^0 = \frac{1}{2}E_{O2} = -4.77$ eV. Similarly, from Eq. (5), the O-poor case corresponds to $\mu_0{}^{Y_2O_3} = \mu_O^0 + 1/3 \times E_{\text{form}}^{Y_2O_3} = -4.77 + 1/3 \times (-19.38) = -11.23$ eV. We have considered O chemical potential in Y_2O_3 ($\mu_O^{Y_2O_3}$) in the full range between the oxygen-rich case and oxygen-poor case as defined above.

To find the formation energy for Y substitutional defect we need the chemical potential of Y in Y_2O_3. From the value of O chemical potential at different T and P and using Eq. (1), it is not possible to find $\mu_Y^{Y_2O_3}$ at different T and P as we do not have the value of $E_{Y_2O_3}$ at different T and P (from DFT, we have $E_{Y_2O_3}$ at ambient condition). So the value of $\mu_Y^{Y_2O_3}$ is taken as a few points in the range $\mu_Y^0 + \frac{1}{2}E_{\text{form}}^{Y_2O_3} < \mu_Y^{Y_2O_3} < \mu_Y^0$. We have considered two limiting values and three intermediate values, e.g, Y rich condition (O poor)μ_Y^0; intermediate values $\mu_Y^0 + \frac{1}{8}E_{\text{form}}^{Y_2O_3}$, $\mu_Y^0 + \frac{1}{4}E_{\text{form}}^{Y_2O_3}$, and $\mu_Y^0 + \frac{1}{3}E_{\text{form}}^{Y_2O_3}$; and Y poor condition (O rich) $\mu_Y^0 + \frac{1}{2}E_{\text{form}}^{Y_2O_3}$.

Figure 8 presents the computed formation energy [65] for interstitial defects (red line), O substitutional defect (green line), and Y substitutional defect (purple line) as a function of O chemical potential (for O substitutional) and Y chemical potential (for Y substitutional). Please note that the x axis for $\mu_O^{Y_2O_3}$ is scaled with $^1/_2 \times E_{O_2}$ as zero reference [63], i.e., the scale is in ($\mu_0{}^{Y_2O_3} - \frac{1}{2}E_{O_2}$). Dotted vertical black lines on the left and right refer to O-poor (low oxygen pressure) and O-rich (high oxygen pressure) cases, respectively. Now, in the scale of ($\mu_0{}^{Y_2O_3} - \frac{1}{2}E_{O_2}$), the O-rich case corresponds to 0 eV ($\mu_0{}^{Y_2O_3} = -4.77$ eV), whereas the O-poor case corresponds to −6.46 eV ($\mu_0{}^{Y_2O_3} = -11.23$ eV). For Y substitutional defect the top axis is the x axis. Please note that there is no one-to-one correspondence between the bottom x axis (O chemical potential) and the top x axis (Y chemical potential), but the O-poor and O-rich lines are in the same direction for both the axes, which is important here. We can see from Fig. 8 that O substitutional defects are favored under O-poor condition (low O_2 pressure) whereas interstitial and Y substitutional defects are favored under O-rich condition (high O_2 pressure). For C doped TiO_2 also O substitutional defects are preferred under low O_2 pressure and interstitial defects are preferred under high O_2 pressure [59]. So our results are consistent with the reported work on C doped oxides. Under atmospheric pressure, interstitial defects are favorable and once O chemical potential reduces below −1.18 eV O substitutional defects start dominating. This is expected as in actual experiment C dopant first sits on the interstitial position and once the O_2 pressure is tuned to a lower value O atoms from Y_2O_3 come out and C occupies the O site. So, to synthesize O substitutional C doped

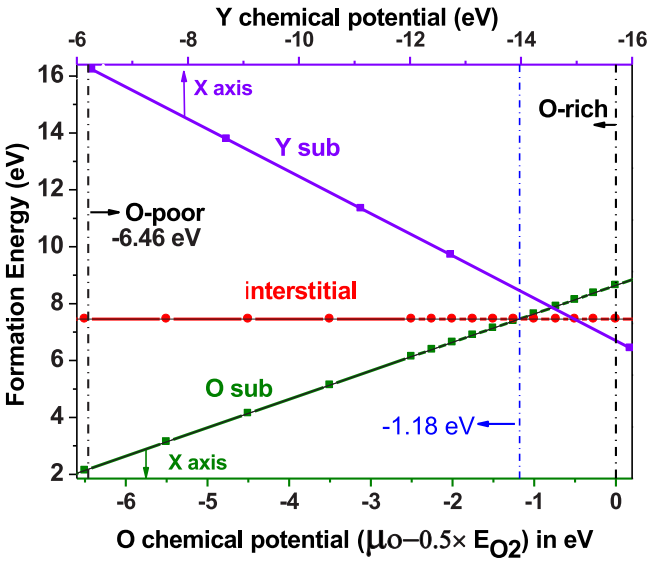

FIG. 8. Computed formation energy for interstitial defects (red line), O substitution defect (green line), and Y substitution defect (purple line) as a function of O chemical potential ($\mu_0 - \frac{1}{2}E_{O2}$) and Y chemical potential (for Y substitution). For Y substitution defect the top axis is the x axis; dotted vertical lines on the left and right refer to O-poor (low oxygen pressure) and O-rich (high oxygen pressure) cases. O substitution defects are favored under O-poor condition ($\mu_o < -1.18$ eV, which may correspond to O_2 pressure of $\sim 10^{-3}$ atm at 800 K, or 10^{-6} atm at 700 K, or 10^{-1} atm at 1000 K).

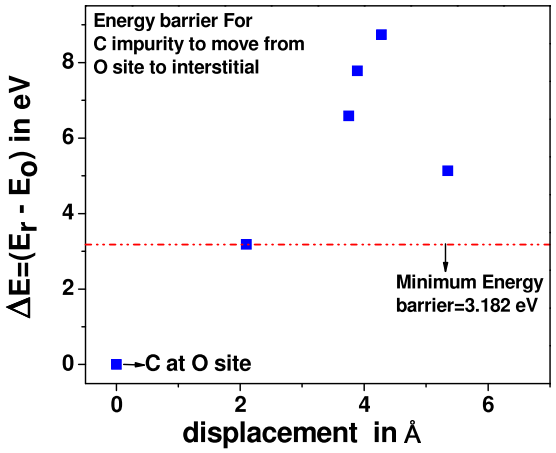

FIG. 9. Diffusion energy barrier for C impurity for moving from the O site towards the interstitial site; in energy barrier $\Delta E = (E_r\text{-}E_O)$, E_O is the energy of the system when the C impurity is at the O site, and E_r is the energy of the system when the C impurity is at the interstitial site (with vacancy at the O site) at a distance r from the O site.

Y_2O_3, O_2 pressure and temperature are required to be tuned such that O chemical potential reduces to below -1.18 eV. Using the equation $\mu_0(T,P) = \mu_0(T,P_0) + \frac{1}{2}KT \times \ln(\frac{P}{P_0})$ and the value of $\mu_0(T,P_0)$ from Ref. [63], we can compute that $\mu_0(T,P) < -1.18$ eV may correspond to O_2 pressure of $\sim 10^{-3}$ atm at 800 K, 10^{-6} atm at 700 K, or 10^{-1} atm at 1000 K. These experimental conditions are very much used and easy to achieve. So stable configuration of O substitutional C doped Y_2O_3 can be synthesized in experiment under low O_2 pressure and high temperature.

Now we will explore whether O substitutional defects formed at low pressure and high temperature are stable at ambient condition or not. Is there a chance that the C atom doped at the O site under low pressure and high T can diffuse to interstitial position at ambient condition? To check this, we have successively moved C atoms from the O site towards the interstitial site (keeping the O site vacant) in small steps and computed the energy for each configuration. In Fig. 9, we have plotted the energy difference, ΔE, between the energies of the system when the C atom is at various interstitial positions (vacancy at that particular O site) and when the C atom is at the O site as a function of displacement of the C atom from the O site. We can notice that there exists an energy barrier for the C atom to diffuse from the O site to the interstitial site at ambient condition. From the set of computed data, the minimum energy barrier is 3.18 eV. This energy barrier stops the C atom from diffusing from the O site to the interstitial site and makes O substitutional defects stable at ambient condition. So, it is feasible to form O substitutional defects in Y_2O_3 by tuning the pressure and temperature and once they are formed they remain stable at ambient condition. The stability of substitutional defects is also seen through *ab initio* MD simulations at room temperature (300 K) as displayed in Fig. 6(c). So, from the formation energy data and MD snapshot at 300 K, we can confidently predict that the most stable defect configuration of a single carbon impurity is the oxygen substitution. The stability of the structure and favorable formation energy infer that it is practically feasible to tailor C doped Y_2O_3 as d^0 FM with a magnetic moment of around 2.0 μ_B per defect at hole concentrations of around 1.63×10^{21} cm^{-3}, with FM coupling large enough to promote room-temperature FM, and the mechanism can be explained in terms of the well-established Stoner criterion.

I. Charged defects

So far, we have presented and analyzed the data for the neutral C defect. From the energy parameters, it was found that C defect at the substitutional site is the most preferred configuration. There may be the possibility that the impurity C may become positively or negatively charged. To study the changes in the spin state and local environment due to charged defect, we have repeated our simulations considering C (single impurity) as positively charged (C^+) and negatively charged (C^-) defect. Figure 10 presents the relaxed structures [Figs. 10(a) and 10(c)] and density of states [Figs. 10(b) and 10(d)] for positively charged defect C^+ (substitutional) and negatively charged defects C^- in yttria with impurity concentration of 2.08 at. %. When C is considered as positively charged (C^+), the magnetic moment per defect increases to 3.0 μ_B compared to 2.0 μ_B for neutral defect, and when C is considered as negatively charged (C^-) the magnetic moment per defect reduces to 1.0 μ_B. These results are quite expected as in this case the origin of ferromagnetism is hole doping and when C is positively charged (C^+) the number of holes per defect increases to 3, resulting in magnetic moment of 3.0 μ_B compared to neutral defect where the number of holes is 2

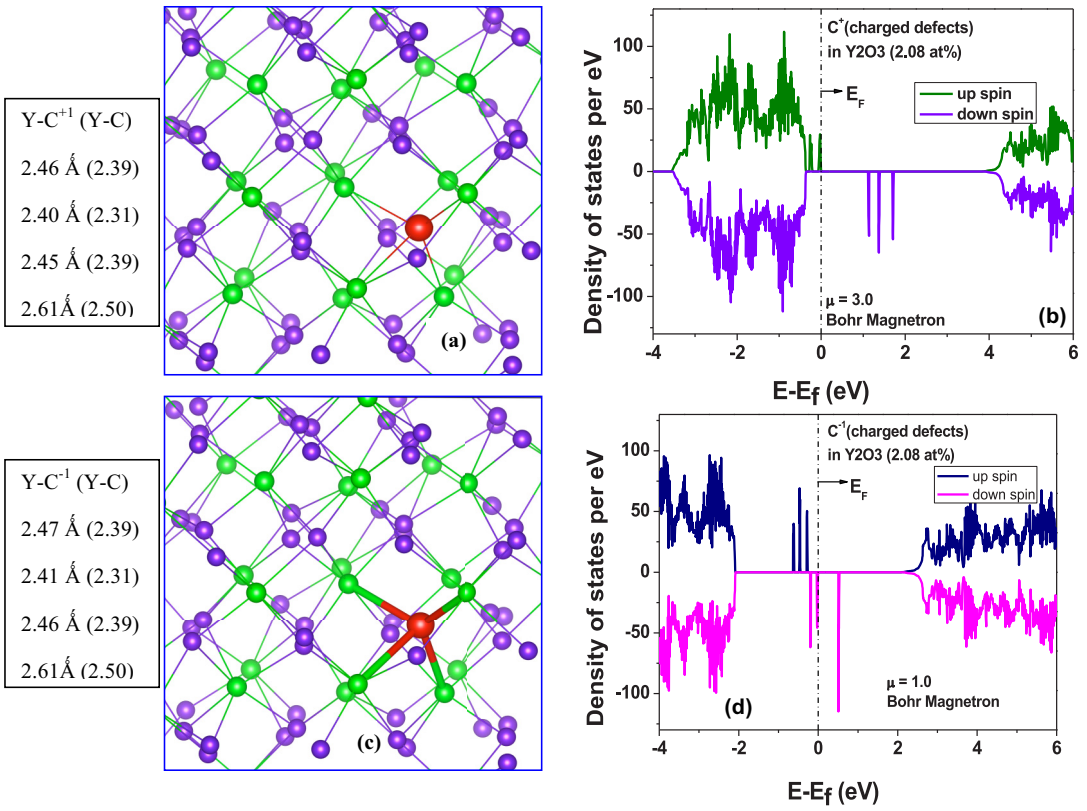

FIG. 10. Relaxed structure and density of states for positively charged defect C^{1+} (substitutional) (a and c) and negatively charged defects C^{1-} (b and d) in yttria with impurity concentration of 2.08 at. %. Green, purple, and red atoms are Y, O, and C, respectively; Y- C^{1+} and Y- C^{-1} bond lengths are also shown and compared with Y-C (neutral) bond length in brackets.

per defect. Similarly, when C is negatively charged (C^-), the number of holes per defect reduces to 1. As far as the local configuration of the defect is concerned, the nearest Y-C^+ (Y-C^-) bond length is increased to 2.40 Å (2.41) from the corresponding Y-C (neutral) bond length of 2.31 Å. There is no change in the symmetry of the structure. The density of states as presented in Figs. 10(b) and 10(d) shows three up-spin and three down-spin impurity levels for both positively charged (C^+) and negatively charged (C^-) defects, similar to neutral C defects in Fig. 2. For positively charged (C^+) defect, all three up-spin impurity levels are fully occupied whereas all three down-spin impurity levels are unoccupied, resulting in a net magnetic moment of 3.0 μ_B. For negatively charged (C^-) defect, all three up-spin impurity levels are fully occupied whereas two down-spin impurity levels are occupied, resulting in a net magnetic moment of 1.0 μ_B. So the system remains in the FM state even with C as charged defects.

IV. CONCLUSIONS

We have performed thorough density functional theory simulations and predict that C doping in nonmagnetic Y_2O_3 leads to room-temperature d^0 ferromagnetism with a magnetic moment of 2.0 μ_B per defect at an impurity concentration of as low as 2.08 at. %. We found a substantial but short-ranged ferromagnetic coupling between C impurities leading to a stable d^0 FM sustained at room temperature. The impurity concentration and distance between the impurity atoms have been varied to study the range of ferromagnetic interactions. Induced magnetic moment computed using GGA exchange-correlation functions has been verified using a state-of-the-art hybrid functional based on the HSE06 functional. The analysis of the partial density of states and spin-density plot signifies that the induced magnetic moment is due to the localized $2p$ orbital of the impurity C and O atoms and the system satisfies the Stoner criteria for ferromagnetism. The persistence of ferromagnetism at room temperature is established through computation of the Curie temperature and *ab initio* MD simulations, which also confirms the stability of the system. We have also investigated the changes in the spin state and local environment due to charged defect by considering C (single impurity) as positively charged (C^+) and negatively charged (C^-) defect. The system remains in the FM state even with C as charged defects with slight elongation of Y-C^+(C^-) bond length compared to Y-C bond length. We strongly believe that room-temperature ferromagnetism in C doped yttria soon will be identified by experiment for the practical realization of DMS.

ACKNOWLEDGMENTS

B.C. would like to thank Dr. N. K. Sahoo for his constant support and encouragements. B.C. would also like to acknowledge help from Bhabha Atomic Research Centre (BARC)'s supercomputing facility and help from Abhijeet Gangan. B.C.

would also like to thank Dr. S. Banerjee for his inspiration and useful scientific discussions. P.K.N. would like to acknowledge Dr. Sharat Chandra from Indira Gandhi Centre for Atomic Research (IGCAR), Kalpakkam and the Centre for Computational Materials Science (CCMS), Institute for Materials Research, Tohoku University, Japan for providing the supercomputing resources that were partially used to perform the simulations presented in this paper.

[1] T. Dietl, H. Ohno, F. Matsukura, J. Cibert, and D. Ferrand, Science **287**, 101 (2000).
[2] S. A. Wolf, D. D. Awschalom, R. A. Buhrman, J. M. Daughton, S. von Molnar, M. L. Roukes, A. Y. Chtchelkanova, and D. M. Tregger, Science **294**, 1488 (2001).
[3] Y. Matsumoto, M. Murakami, T. Shono, T. Hasegawa, T. Fukumara, M. Kawasaki, P. Ahmet, T. Chikyow, S.-Y. Koshihara, and H. Koinuma, Science **291**, 854 (2001).
[4] S. A. Chambers, S. Thevuthasan, R. F. C. Farrow, R. F. Marks, J. U. Thiele, L. Folks, M. G. Samant, A. J. Kellock, N. Ruzycki, D. L. Ederer, and U. Diebold, Appl. Phys. Lett. **79**, 3467 (2001).
[5] H.Y. Xu, Y. C. Liu, Y. X. Liu, C. S. Zhu, C. L. Shao, and R. Mu, Appl. Phys. Lett. **88**, 242502 (2006).
[6] J. H. Park, M. G. Kim, H. M. Jang, and S. W. Ryu, Appl. Phys. Lett. **84**, 1338 (2004).
[7] H. Pan, J. B. Yi, L. Shen, R. Q. Wu, J. H. Yang, J. Y. Lin, Y. P. Feng, J. Ding, L. H. Van, and J. H. Yin, Phys. Rev. Lett. **99**, 127201 (2007).
[8] A. M. Stoneham, A. P. Pathak, and R. H. Bartram, J. Phys. C **9**, 73 (1976).
[9] I. S. Elfimov, S. Yunoki, and G. A. Sawatzky, Phys. Rev. Lett. **89**, 216403 (2002).
[10] G. Rahman, V. M. García-Suárez, and S. C. Hong, Phys. Rev. B **78**, 184404 (2008).
[11] G. Bouzerar and T. Ziman, Phys. Rev. Lett. **96**, 207602 (2006).
[12] B. Chakraborty and L. M. Ramaniah, J. Magn. Magn. Mater. **385**, 207 (2015).
[13] J. B. Yi, C. C. Lim, G. Z. Xing, H. M. Fan, L. H. Van, S. L. Huang, K. S. Yang, X. L. Huang, X. B. Qin, B. Y. Wang, T. Wu, L. Wang, H. T. Zhang, X. Y. Gao, T. Liu, A. T. S. Wee, Y. P. Feng, and J. Ding, Phys. Rev. Lett. **104**, 137201 (2010).
[14] S. Chawla, K. Jayanthi, and R. K. Kotnala, Phys. Rev. B **79**, 125204 (2009).
[15] L. X. Guan, J. G. Tao, C. H. A. Huan, J. L. Kuo, and L. Wang, J. Appl. Phys. **108**, 093911 (2010).
[16] F. Máca, J. Kudrnovský, V. Drchal, and G. Bouzerar, Appl. Phys. Lett. **92**, 212503 (2008).
[17] W. Zhou, L. Liu, and P. Wu, J. Magn. Magn. Mater. **321**, 3356 (2009).
[18] K. Kenmochi, M. Seike, K. Sato, A. Yanase, and H. Katayama-Yoshida, Jpn. J. Appl. Phys. **43**, L934 (2004).
[19] K. Kenmochi, V. A. Dinh, K. Sato, A. Yanase, and H. Katayama-Yoshida, J. Phys. Soc. Jpn. **73**, 2952 (2004).
[20] I. S. Elfimov, A. Rusydi, S. I. Csiszar, Z. Hu, H. H. Hsieh, H.-J. Lin, C. T. Chen, R. Liang, and G. A. Sawatzky, Phys. Rev. Lett. **98**, 137202 (2007).
[21] H. Wu, A. Stroppa, S. Sakong, S. Picozzi, M. Scheffler, and P. Kratzer, Phys. Rev. Lett. **105**, 267203 (2010).
[22] S. Zhou, Q. Xu, K. Potzger, G. Talut, R. Grötzschel, J. Fassbender, M. Vinnichenko, J. Grenzer, M. Helm, H. Hochmuth, M. Lorenz, M. Grundmann, and H. Schmidt, Appl. Phys. Lett. **93**, 232507 (2008).
[23] L. Liu, L. Wang, Y. Li, C. Zhang, Y. Cho, S. Wing, T. Zhou, T. Taked, N. Hirosakib, and R.-J. Xie, J. Mater. Chem. C **5**, 8927 (2017).
[24] Y. Wang, Y. Liu, G. Wang, W. Anwand, C. A. Jenkins, E. Arenholz, F. Munnik, O. D. Gordan, G. Salvan, D. R. T. Zahn, X. Chen, S. Gemming, M. Helm, and S. Zhou, Sci. Rep. **5**, 8999 (2014).
[25] M. Zhao, F. Pan, and L. Mei, Appl. Phys. Lett. **96**, 012508 (2010).
[26] P. Lou, RSC Adv. **6**, 39595 (2016).
[27] Y. Kopelevich, R. R. De Silva, J. H. S. Torres, A. Penicaud, and T. Kyotani, Phys. Rev. B **68**, 092408 (2003).
[28] A. V. Rode, E. G. Gamaly, A. G. Christy, J. G. Fitz Gerald, S. T. Hyde, R. G. Elliman, B. Luther-Davies, A. I. Veinger, J. Androulakis, and J. Giapintzakis, Phys. Rev. B **70**, 054407 (2004).
[29] P. Esquinazi, D. Spemann, R. Höhne, A. Setzer, K.-H. Han, and T. Butz, Phys. Rev. Lett. **91**, 227201 (2003).
[30] S. Talapatra, P. G. Ganesan, T. Kim, R. Vajtai, M. Huang, M. Shima, G. Ramanath, D. Srivastava, S. C. Deevi, and P. M. Ajayan, Phys. Rev. Lett. **95**, 097201 (2005).
[31] H. Ohldag, T. Tyliszczak, R. Höhne, D. Spemann, P. Esquinazi, M. Ungureanu, and T. Butz, Phys. Rev. Lett. **98**, 187204 (2007).
[32] P. O. Lehtinen, A. S. Foster, A. Ayuela, T. T. Vehviläinen, and R. M. Nieminen, Phys. Rev. B **69**, 155422 (2004).
[33] P. Deák, B. Aradi, T. Frauenheim, E. Janzén, and A. Gali, Phys. Rev. B **81**, 153203 (2010).
[34] J. Heyd, G. E. Scuseria, and M. Ernzerhof, J. Chem. Soc. **132**, 2876 (2010).
[35] G. Kresse and J. Hafner, Phys. Rev. B **47**, 558(R) (1993).
[36] G. Kresse and J. Hafner, Phys. Rev. B **49**, 14251 (1994).
[37] G. Kresse and J. Furthmüller, Comput. Mater. Sci. **6**, 15 (1996).
[38] G. Kresse and J. Furthmüller, Phys. Rev. B **54**, 11169 (1996).
[39] J. P. Perdew, J. A. Chevary, S. H. Vosko, K. A. Jackson, M. R. Pederson, D. J. Singh, and C. Fiolhais, Phys. Rev. B **46**, 6671 (1992).
[40] M. Bühl, C. Reimann, D. A. Pantazis, T. Bredow, and F. Neese, J. Chem. Theo. Compu. **4**, 1449 (2008).
[41] J. H. Monkhorst and J. D. Pack, Phys. Rev. B **13**, 5188 (1976).
[42] S. Nose, Mol. Phys. **52**, 255 (1984).
[43] R. W. G Wyckoff, *Crystal Structure* (Interscience, New York, 1996).
[44] D. R. Mueller, D. L. Ederer, J. van Ek, W. L. O'Brien, Q. Y. Dong, J. Jia, and T. A. Callcott, Phys. Rev. B **54**, 15034 (1996).
[45] P. W. Robertson and J. Peacock, J. Appl. Phys. **92**, 4712 (2002).
[46] J. H. Jeong, J. S. Bae, S.-S. Yi, J.-C. Park, and Y. S. Kim, J. Phys.: Condens. Matter **15**, 567 (2003).
[47] B. Chakraborty and L. M. Ramaniah, J. Phys.: Condens. Matter **28**, 336001 (2016).

[48] Y. J. Zhao, T. Shishidou, and A. J. Freeman, Phys. Rev. Lett. **90**, 047204 (2003).
[49] L. H. Ye, A. J. Freeman, and B. Delley, Phys. Rev. B **73**, 033203 (2006).
[50] J. Osorio-Guillen, S. Lany, S. V. Barabash, and A. Zunger, Phys. Rev. Lett. **96**, 107203 (2006).
[51] J. Kudrnovský, I. Turek, V. Drchal, F. Máca, P. Weinberger, and P. Bruno, Phys. Rev. B **69**, 115208 (2004).
[52] G. Bouzerar, J. Kudrnovský, L. Bergqvist, and P. Bruno, Phys. Rev. B **68**, 081203(R) (2003).
[53] H. Peng, H. J. Xiang, S.-H. Wei, S.-S. Li, J.-B. Xia, and J. Li, Phys. Rev. Lett. **102**, 017201 (2009).
[54] P. Dev and P. Zhang, Phys. Rev. B **81**, 085207 (2010).
[55] W.Q. Li, J. X. Cao, J. W. Ding, and X. Hu, J. Appl. Phys. **110**, 123908 (2011)
[56] J. X. Zheng, G. Ceder, T. Maxisch, W. K. Chim, and W. K. Choi, Phys. Rev. B **73**, 104101 (2006).
[57] J. G. Speight, *Lange's Handbook of Chemistry*, 16th ed. (McGraw-Hill, New York, 2005).
[58] N. Berseneva, A. V. Krasheninnikov, and R. M. Nieminen, Phys. Rev. Lett. **107**, 035501 (2011).
[59] C. Valentin, G. Pacchioni, and A. Selloni, Chem. Mater. **17**, 6656 (2005).
[60] J. Lu, Y. Dai, M. Guo, L. Yu, K. Lai, and B. Huang, Appl. Phys. Lett. **100**, 102114 (2012).
[61] J Atanelov, C. Gruber, and P. Mohn, Comput. Mater. Sci. **98**, 42 (2015).
[62] X. L. Sheng, H. J. Cui, F. Ye, Q. B. Yan, Q. R. Zheng, and G. Su, J. Appl. Phys. **112**, 074315 (2012).
[63] K. Reuter and M. Scheffler, Phys. Rev. B **65**, 035406 (2001).
[64] H. Choi, S. H. Cho, S. Khan, K.-R. Lee, and S. Kim, J. Mater. Chem. C **2**, 6017 (2014).
[65] S. B. Zhang and J. E. Northrup, Phys. Rev. Lett. **67**, 2339 (1991).